Pergamon

Int. J. Heat Mass Transfer. Vol. 37, No. 14, pp. 2155–2163, 1994

0017-9310/94 $7.00+0.00

0017-9310(93)E0119-2

Investigation of heat and mass transfer in the evaporation zone of a heat pipe operating by the 'inverted meniscus' principle

A. S. DEMIDOV
Department of Mechanics and Mathematics, Moscow State University, Moscow 119899, Russia

and

E. S. YATSENKO
The All-Union Electrotechnic Institute, Istra, Moscow Region 143500, Russia

(*Received* 12 *August* 1993)

Abstract—A theoretical investigation of heat and mass transfer during evaporation in a wet capillary structure in contact with a heating wall is presented. The wall has grooves by which the vapour is removed. Setting and results of the numerical investigation of the mathematical model (stationary two-dimensional boundary problem with a free boundary corresponding to the surface of the interphase transition inside the capillary structure) are given. Calculations performed at different heat and hydraulic loads allow one to trace the phases of the process evolution: origin and growth of vapour zones (bubbles). The evaporation intensity distribution and functional characteristic of the capillary structure have been found.

1. INTRODUCTION

THE PROBLEM described below arose from consideration of heat and mass transfer and evaporation processes in heat pipe wicks [1]. A wick is a layer of a capillary structure (CS). The inner side of the wick is in contact with a hot wall with a grooved surface (Fig. 1); its outer side is cooled by a liquid. Vapour is removed by the grooves on the surface of the heating wall. The capacity of the wick is determined by the processes occurring inside the CS near microcontacts with the heating wall. These salients act as heat input elements (HIE) for the CS. This paper, previously presented in part in refs. [2–4], is devoted to a theoretical investigation of this problem.

A single microcontact [5] can operate in the following two typical conditions: (a) when the vapour zone is 'large' (Fig. 2a), i.e. it exceeds the zone of contact with HIE and touches the corner point A, and (b) when the vapour zone is 'small' (Fig. 2b), that is either non-existent or not exceeding the zone of contact with HIE on the surface of the CS; in this case there is a meniscus of liquid near the corner point A.

The operating conditions presented in Fig. 2(b) are typical for small vapour pressure differences at its discharge from the CS. However, high intensity of evaporation may be obtained also in those conditions, since the meniscus of liquid takes an active part in the evaporation.

An important observation is that heat and mass transfer in the structures under consideration is essentially not one-dimensional, since the heat flux from the HIE spreads and curves inside the CS and flows out together with the steam, circulating the areas of microcontact between the CS and the HIE.

2. PROBLEM STATEMENT

This paper considers the boundary problem with transmission (conjugation) conditions on a free boundary for energy system equations, motion (in Darcy form) and continuity in a region, Ω, corresponding to the CS cross-section fragment (the rectangle $OBCD$ in Fig. 3) in the area of its contact with one of the HIEs. The unknown curve (free boundary) γ divides the region Ω into two subregions: 'wet' Ω^-

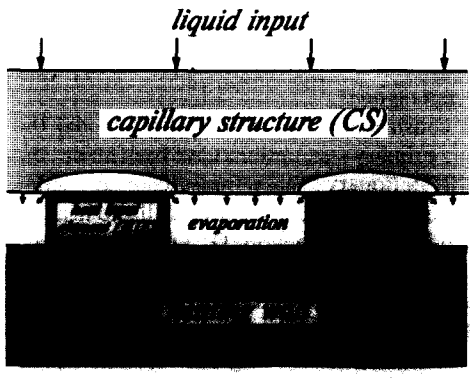

FIG. 1. The scheme of evaporation in a CS.

NOMENCLATURE

CS capillary structure
HIE heat input element
I intensity of evaporation (evaporation rate)
K coefficient of permeability
R radius of meniscus
T temperature
$T_{-\infty}$ temperature of the input liquid
$\bar{T}_c$ integral average temperature on Γ_c
$T_* = \bar{T}_c - T_\infty$ thermal action upon the CS
T_*^0 thermal action, corresponding to the transition from a 'small' to a 'large' vapour zone
$\mathbf{V}$ working fluid motion rate (velocity of the heat carrier)
$a = \rho c K/\mu\lambda$ [cf. equation (2)]
c specific heat capacity
d CS capillaries size
h difference mesh width
j iteration parameter in Richardson method
k_f 'forestalling' coefficient
l_h distance between $\gamma_h^\pm$ and γ
n iteration number of the solution to problem (1)–(21)
p pressure
p_A pressure of corner point A (Figs. 3 and 4)
p_c pressure jump on γ
$p_S(T)$ saturation pressure
q heat flux
r specific heat of vaporisation
$u = (p_{n+1}, T_{n+1})$ nth iteration of the solution of problem (1)–(21)
u_j jth iteration of u
u_j^h numerical approximation of u_j
$v_j = (\pi, \tau)$ solution of problem (24)–(27)
x, y Cartesian coordinate axes.

Greek symbols
$\Gamma_c, \Gamma_e, \Gamma_H, \Gamma_l, \Gamma_0, \Gamma_s, \Gamma_v, \Gamma_x^m, \Gamma_v^m$ sections of the boundary of the region $\Omega \cup \Omega_H$ (cf. Fig. 3)
Ω region corresponding to the CS cross-section fragment
α coefficient of heat convective transfer
γ free boundary, a part of the liquid–vapour interphase boundary within the capillary structure
δ_Q distance from the point Q to the meniscus surface
ν, η coordinates corresponding to the normal and tangent to γ
ε decrement of the initial residual
θ edge angle of wetting (boundary wetting angle)
λ coefficient of the effective thermal conductivity of the CS
μ coefficient of dynamic viscosity
ρ density of the working fluid flowing in the CS
σ surface tension factor
ω_h curvilinear strip.

Superscripts
$+, -$ indicate that the region or boundary ($\Omega^\pm, \gamma^\pm, \gamma_h^\pm$) is either wet or dry, respectively.

Subscripts
H corresponds to heat ($\Omega_H, \lambda_H, \Gamma_H, T_H$)
l corresponds to liquid (Γ_l, p_l, λ_l)
n corresponds to the nth iteration (p_n, T_n, γ_n)
∞ corresponds to region at a distance from the evaporation section (p_∞, T_∞).

and 'dry' Ω^+. The boundary γ corresponds to that part of the interphase boundary which lies inside the CS.

2.1. *Assumptions*

In constructing the mathematical model the following primary assumptions have been made: the process is stationary; mass forces changes within the region under consideration are small; no heat sources or drains inside the regions Ω^- and Ω^+ are available; the CS is isotropic; there is a local temperature balance between the CS and the working fluid contained in it; convective heat exchange is negligible in comparison with that occurring by evaporation; vapor is incompressible.

2.2. *Differential equations*

According to the assumptions made, the considered equations of energy, motion and continuity are of the following form

$$\lambda \Delta T = \rho c(\mathbf{V}, \nabla T), \quad \mathbf{V} = -\frac{K}{\mu}\nabla p, \quad \operatorname{div}\mathbf{V} = 0,$$

where $\nabla = \operatorname{grad}$, $\Delta = \partial^2/\partial x^2 + \partial^2/\partial y^2$ is the Laplacian operator, T is the temperature, $\mathbf{V}$ is the working fluid motion rate and p is the pressure. The letters ρ, c and μ denote, respectively, density, specific heat capacity and coefficient of dynamic viscosity of the working fluid flowing in the CS; λ is the coefficient of the effective thermal conductivity of the CS, containing the working fluid [6]; K is the coefficient of its per-

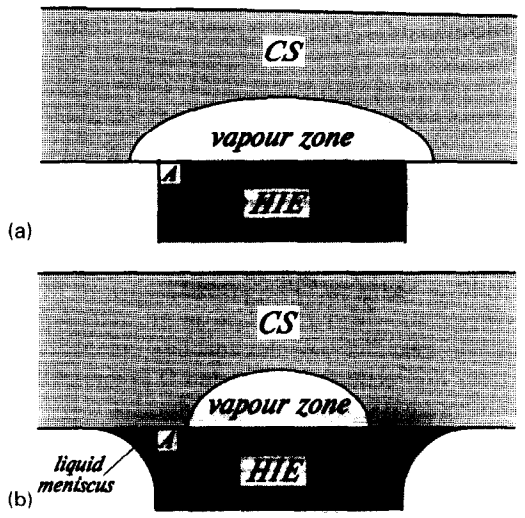

FIG. 2. An isolated microcontact of HIE and CS: (a) with 'large' vapour zone, (b) with 'small' vapour zone.

meability. Generally, the values of the coefficients are different for the Ω^- and Ω^+ subregions.

Potentiality and solenoidality of the rate field $\mathbf{V}$ allow the above system of equations to be written in the form of the differential equations system

$$\Delta p = 0 \quad \text{in}\,\Omega \tag{1}$$

$$\Delta T + a\cdot(\nabla p, \nabla T) = 0 \quad \text{in}\,\Omega, \quad a = \frac{\rho c K}{\mu\lambda} \tag{2}$$

for pressure $p = p(x, y)$ and temperature field $T = T(x, y)$.

2.3. *Boundary and transfer conditions*

The equation system (1), (2) is supplemented by the boundary conditions at the $OBCD$ rectangle boundary (Fig. 3) and transmission conditions on the boundary γ.

Heat drain on boundary γ is considered as a heat flux at the jump equivalent to the mass flux flowing through γ: therefore

$$\lambda\frac{\partial T}{\partial v}\bigg|_{\gamma^+} - \lambda\frac{\partial T}{\partial v}\bigg|_{\gamma^-} = -\frac{\rho r K}{\mu}\frac{\partial p}{\partial v}\bigg|_{\gamma}, \tag{3}$$

where r is specific heat of vaporization, $\partial/\partial v$ is the differential operator along the normal $\mathbf{v}$ to γ, and $f|_{\gamma^+}$ designates the boundary value of the function f on the curve γ from the side of the region Ω^+. The second condition on the boundary γ reflects the mass flux balance

$$\frac{\rho r K}{\mu}\frac{\partial p}{\partial v}\bigg|_{\gamma^+} - \frac{\rho r K}{\mu}\frac{\partial p}{\partial v}\bigg|_{\gamma^-} = 0. \tag{4}$$

The third transmission condition

$$p|_{\gamma^+} - p|_{\gamma^-} = p_c \tag{5}$$

on the boundary γ allows for the capillary forces in the form of the pressure jump across the boundary γ.

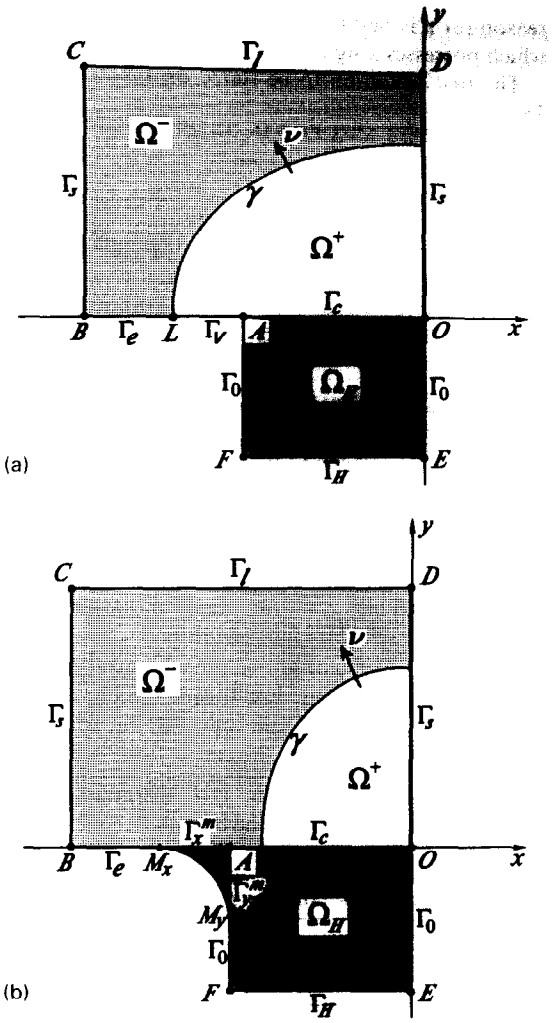

FIG. 3. The area of calculations corresponding for a fragment of a CS cross-section at the point of its contact with the HIE: (a) with 'large' vapour zone; (b) with 'small' vapour zone. The regions Ω^- and Ω^+ correspond, respectively, to the liquid phase and the vapour phase of the heat carrier; the region Ω_H corresponds to an HIE; $\Gamma_H = EF$ is the section of heat input into Ω_H; $\Gamma_c = OA$ is the section of contact between the CS and HIE; Γ_0 is the vertical parts of the boundary of Ω_H free from meniscus, i.e. $\Gamma_0 = OE \cup AF$ in case (a) and $\Gamma_0 = OE \cup M_yF$ in case (b); $\Gamma_x^m = AM_x$ and $\Gamma_y^m = AM_y$ are bases of the meniscus; Γ_s is the vertical lines OD and BC with respect to which pressure and temperature are symmetric; $\Gamma_f = CD$ is the section of liquid input into the region Ω; Γ_e is the evaporation section, i.e. the part of interphase boundary, lying on the surface of the CS; $\Gamma_c = BL$ in case (a) and $\Gamma_c = BM_x$ in case (b); $\Gamma_v = AL$ is the section of vapour discharge from the vapour zone (Fig. 3a).

This jump is constant and equal to the CS capillary head, i.e. $p_c = (4\sigma\cos\theta)/d$, where σ is the surface tension coefficient, θ is the edge angle of wetting, and d is the CS capillary size. The final condition of transmission

$$T|_{\gamma^+} - T|_{\gamma^-} = 0 \tag{6}$$

represents the temperature jump absence on γ. The

reason for it is that the boundary γ lies inside the CS, which possesses a significant thermal conductance.

The first condition to be stated on $\Gamma_c = OA$ (Fig. 3) is

$$\frac{\partial p}{\partial y} = 0 \quad \text{on } \Gamma_c \tag{7}$$

which reflects the wall's inpermeability for the mass flux. The condition of heat input to region Ω through Γ_c is modelled by introducing the additional region Ω_H corresponding to the HIE tooth cross-section. In Ω_H the stationary temperature fluid satisfies the Laplace equation

$$\Delta T = 0 \quad \text{in } \Omega_H . \tag{8}$$

With regard to this the heat input into the region Ω is described by the transmission conditions on Γ_c in the form of the temperature jump absence at the transition from Ω_H to Ω, i.e.

$$T(x,y)|_{y=+0} - T(x,y)|_{y=-0} = 0 \quad \text{at } (x,0) \in \Gamma_c \tag{9}$$

and heat flux equality, i.e.

$$\lambda \frac{\partial T}{\partial y}(x,y)|_{y=+0} = \lambda_H \frac{\partial T}{\partial y}(x,y)|_{y=-0} \quad \text{at } (x,0) \in \Gamma_c , \tag{10}$$

where λ_H is coefficient of the HIE thermal conductivity. On $\Gamma_H = EF$ (Fig. 3) the boundary condition is stated as

$$T = T_H = \text{const} > T_\infty \quad \text{on } \Gamma_H , \tag{11}$$

where T_∞ is the vapour temperature at a distance from the evaporation section Γ_e. On the vertical parts of the edge of the region Ω_H free from meniscus, the condition of heat exchange absence is stated as

$$\frac{\partial T}{\partial x} = 0 \quad \text{on } \Gamma_0 , \tag{12}$$

where $\Gamma_0 = OE \cup AF$ in the case shown in Fig. 3(a), and $\Gamma_0 = OE \cup FM_y$ with the meniscus present (Fig. 3b). The condition (12) follows from the supposed negligibility of the convective heat exchange in comparison with heat exchange during evaporation and symmetry of the temperature field with respect to the OE segment.

The conditions of heat and mass transfer on the evaporation section Γ_e, i.e. on the section of the interphase boundary that lies on the surface of the CS (see Fig. 3), should be stated in the same way as on the boundary via the related transmission conditions, with imposition at the same time of boundary conditions for p and T at a distance from the section Γ_e. Nevertheless, these boundary conditions depend on a particular constructive solution for removal of vapour, whereas allowing for such particularities makes it necessary to consider a three-dimensional problem. In order to avoid these complications and to remain within the frame of a two-dimensional problem, we decided to confine ourselves temporarily to consideration of the following heat transfer condition on Γ_e:

$$\lambda \frac{\partial T}{\partial y} = \alpha (T - T_\infty) \quad \text{on } \Gamma_e , \tag{13}$$

where α is the coefficient of convective heat transfer for evaporation from the micromenisci building up the section Γ_e [6]. The second condition

$$\lambda \frac{\partial T}{\partial y} = \frac{\rho r K}{\mu} \frac{\partial p}{\partial y} \quad \text{on } \Gamma_e \tag{14}$$

reflects the heat and mass flux equality.

At the top section of the region Ω boundary the conditions are stated as

$$p = p_l = \text{const} \quad \text{on } \Gamma_l \tag{15}$$

$$-\lambda \frac{\partial T}{\partial y} = \frac{\rho c K}{\mu} \frac{\partial p}{\partial y} (T - T_\infty) \quad \text{on } \Gamma_l , \tag{16}$$

where p_l is the given pressure on Γ_l, and T_∞ is the temperature of the cooling liquid at a distance from Γ_l. Condition (16) presents the heat balance across the boundary: heat flux flowing from region Ω returns back to it as enthalpy flowing to region Ω^-.

At the vertical parts of the boundary of the region Ω designated as Γ_s (Fig. 3) symmetry conditions are given:

$$\frac{\partial p}{\partial x} = 0 \quad \text{on } \Gamma_s \tag{17}$$

$$\frac{\partial T}{\partial x} = 0 \quad \text{on } \Gamma_s . \tag{18}$$

As to the boundary conditions on the remaining sections of the boundary of the region Ω, they depend on the case considered: with or without meniscus (Fig. 3a, b).

First of all let us consider the case without meniscus. Here, on section Γ_v of vapour output from the vapour zone the conditions are stated as

$$\frac{\partial T}{\partial y} = 0 \quad \text{on } \Gamma_v \tag{19a}$$

$$p = p_\infty = \text{const} \quad \text{on } \Gamma_v . \tag{20a}$$

Here p_∞ is the pressure of vapour leaving the CS. Condition (19a) represents the absence of phase changes (transformations) or other heat drains. As it was noted, the convective heat exchange is negligible compared to that at the adjacent section Γ_e. Condition (20a) shows the acoustic effect exceeding the vapour outflow rate.

In the presence of a meniscus the situation becomes more complicated. Strictly speaking, one should write the differential equations and boundary conditions that describe both the process of heat and mass transfer inside the meniscus and evaporation process from its surface and the meniscus shape itself (i.e. the region it occupies). Such a problem is of particular interest. However, the aim of this paper is to investigate the behaviour of vapour inside a CS, so the influence of

the meniscus is evaluated only qualitatively here. We assume that there is no motion of liquid inside the meniscus, while the meniscus itself is symmetric and its shape can be described as an arc of the circle with the radius

$$R = 2\sigma(\cos\theta)/(p_\infty - p_A),$$

where σ, θ and p_∞ were defined above, and p_A is the pressure at the corner point A. These assumptions allow us to evaluate the influence of the meniscus on evaporation 'from below'. Actually, the motion of liquid within the meniscus will result in some increase in evaporation intensity from its surface.

A meniscus affects the heat and mass transmission in two ways. On the one hand it reduces the heat release from the boundary $\Gamma_x^m = AM_x$, since evaporation takes place not from this boundary but from the meniscus surface, and the heat flux has to overcome the thermal resistance of the liquid. On the other hand the meniscus takes an active part in evaporation; the liquid seeping into it through Γ_x^m evaporates from its surface. The heat fluxes from both Γ_x^m and $\Gamma_y^m = AM_y$ are responsible for this. At the point Q, belonding to Γ_x^m or Γ_y^m and situated at the distance $|AQ|$ from the corner point A

$$\lambda\frac{\partial T}{\partial y} = \alpha_Q(T - T_\infty) \quad \text{for } Q \in \Gamma_x^m$$

and

$$\lambda_H\frac{\partial T}{\partial x} = \alpha_Q(T - T_\infty) \quad \text{for } Q \in \Gamma_y^m, \qquad (19b)$$

where $\alpha_Q = (1/\alpha + \delta_Q/\lambda_l)^{-1}$, δ_Q is the distance between the point Q and the meniscus surface, and λ_l is the coefficient of the liquid's thermal conductivity. In our simplified approach the balance of heat and mass fluxes during evaporation from the meniscus surface is expressed by the following equality:

$$\frac{\lambda_H}{|AM_y|}\int_{\Gamma_y^m}\frac{\partial T}{\partial x}\,dy + \lambda\frac{\partial T}{\partial y}\bigg|_{\Gamma_x^m} = \frac{\rho r K}{\mu}\frac{\partial p}{\partial y} \quad \text{on } \Gamma_x^m. \qquad (20b)$$

2.4. *Condition specifying the free boundary*

Relations (1)–(20) could be considered as a properly (correctly) defined boundary-value problem for the elliptical system of equations with transmission conditions on γ [7] if the boundary γ were known beforehand. However, the conditions (1)–(20) do not specify it. *A priori* it is not given, it is 'free' [8] and can be defined only from an additional condition. The following equality can be taken as the above condition here:

$$p|_{\gamma^+} = p_S(T)|_\gamma, \qquad (21)$$

where $p_s(T)$ is the saturation pressure which is the known to be a strictly increasing function of T. The condition (21) is due to the fact that vapour is saturated and its temperature is close to the temperature of the liquid near the boundary γ. Therefore, the vapour pressure on the boundary γ is equal to saturation pressure.

3. NUMERICAL ALGORITHM SCHEME

The problem (1)–(21) has two special features: (1) the boundary γ is unknown and (2) the transmission conditions are to be satisfied on γ.

These two features, the second of which presents the greatest difficulty by of solution by numerical problem, were dealt with by separating into the algorithm presented below. Namely, the numerical solution of the problem (1)–(21) is reduced to the solution of a sequence of problems (1)–(20) for $p = p_n(x, y)$ and $T = T_n(x, y)$ functions with iteratively defined boundaries γ_n, where $n \geqslant 0$. In this case curves γ_n converged to curve γ, which does not depend on the initial curve γ_0 (arbitrary enough). Even the 'curve' contracted to a point can be taken as γ_0. It corresponds to the fact that at the initial step $\Omega = \Omega^-$. In this case the transmission conditions are absent and $p = p_0(x, y)$ and $T = T_0(x, y)$ initial functions are approximated by any standard numerical method. Richardson's method with Lebedev–Phinogenov [9] modification was used for this purpose. This iteration method of the difference equation solving converges fairly quickly. The initial residual decreases by $1/\varepsilon$ times for the iteration number of $(1/h)\ln(1/\varepsilon)$ order, where h is the difference mesh width. The most important thing is that this method is easily adapted for any geometry of the region in which the elliptical boundary-value problem is considered.

Once the boundary γ_n ($n \geqslant 0$) and p_n and T_n, the corresponding functions, have been found the curve γ_{n+1} is found [cf. equation (21)] from relation

$$p_n|_{\gamma_{n+1}^+} = p_S(T_n)|_{\gamma_{n+1}}. \qquad (22)$$

Although the proof of the existence and uniqueness theorem is beyond the scope of this paper, nevertheless, using the numerical calculations performed, one can speak with certainty of both the existence and the uniqueness of the curve γ_{n+1} being defined by relation (22) and of the existence of a unique solution to initial problem (1)–(21).

After the curve γ_{n+1} is found one can start looking for the solution to problem (1), (2) with transmission condition on $\gamma = \gamma_{n+1}$. This solution is a vector-function $u = (p_{n+1}, T_{n+1})$ which can be represented (cf. ref. [10]) both in terms of

$$\lim_{h\to 0}\lim_{j\to\infty} u_j^h,$$

and in terms of

$$\lim_{j\to\infty} u_j, \quad \text{where } u_j = \lim_{h\to 0} u_j^h.$$

Here h is the difference mesh width, $j \geqslant 0$ is the iteration parameter in Richardson method, and the function u_j is the solution (at the jth iteration, $j \geqslant 1$) of the boundary-value problem in $\Omega = \Omega^+ \cup \Omega^-$ defined by

(1), (2), (7)–(20) and

$$u_j|_{\gamma^\pm} = v_j|_{\gamma^\pm}, \tag{23}$$

where the vector-function v_j is found by the method described below with respect to the function u_{j-1}. In this case as the initial vector-function u_0 one can take the solution of the boundary-value problem in $\Omega = \Omega^+ \cup \Omega^-$ being defined by relations (1), (2), (7)–(20) together with the condition of continuous differentiability on $\gamma = \gamma_{n+1}$.

As to the function v_j, it is defined on the curvilinear stripe ω_h, which is restricted by the curves $\gamma_h^\pm$ lying in $\Omega^\pm$ and at a distance l_h of order h from γ. In ω_h the coordinates (ν,η) corresponding to the normal and tangent to γ are introduced. In these coordinates vector-function v_j, with components π and τ, depending upon η as a parameter, is found explicitly as the solution of the following [cf. equations (1)–(6)] boundary problem for the system of ordinary differential equations with respect to the $\nu \in [l_{-h}, l_h]$ with transmission conditions at $\nu = 0$

$$\pi'' = 0, \quad \tau'' + a \cdot \pi' \cdot \tau' = 0 \quad \text{at } 0 < |\nu| < h \tag{24}$$

$$\pi - p_{j-1} = 0 \quad \text{and} \quad \tau - T_{j-1} = 0$$

$$\text{on} \quad \gamma_h^\pm = \{(\nu,\eta) | \nu = \pm h\} \tag{25}$$

$$\pi|_{\gamma^+} - \pi|_{\gamma^-} = p_c, \quad \frac{\rho r K}{\mu}\pi'|_{\gamma^+} - \frac{\rho r K}{\mu}\pi'|_{\gamma^-} = 0 \tag{26}$$

$$\tau|_{\gamma^+} - \tau|_{\gamma^-} = 0, \quad \lambda\tau'|_{\gamma^+} - \lambda\tau'|_{\gamma^-} = -\frac{\rho r K}{\mu}p'|_{\gamma^-}. \tag{27}$$

In equations (24)–(27) the prime denotes differentiation with respect to ν.

The above algorithm has been improved during the calculations in two ways. First, instead of relation (23) the following condition

$$u_j|_{\gamma^\pm} = k_j v_j|_{\gamma^\pm}$$

was used with specially selected 'forestalling' coefficients k_j. Due to this the convergence rate was increased by one order. Second, near the corner point A, where the mass flux line closeness is observed (Fig. 4), the calculations were performed with a smaller step. In this case transitions between the small mesh zone and that with a larger mesh were inscribed in a basic iteration algorithm and performed just as in the Schwartz alternating method [11, Chap. IV].

4. NUMERICAL CALCULATION RESULTS

The calculations were performed for the CS in the form of sintered copper powder with a capillary size from $d = 4$ to 10 μm and a permeability of $K = 10^{-13}$ m. The thermal properties of the heat transfer agent were in conformity with those of water, the boundary angle of wetting, θ, was assumed to be zero. The effective thermal conductivity was assumed to be $\lambda = 25$ W m^{-1} K^{-1} both in Ω^- and in Ω^+. It was

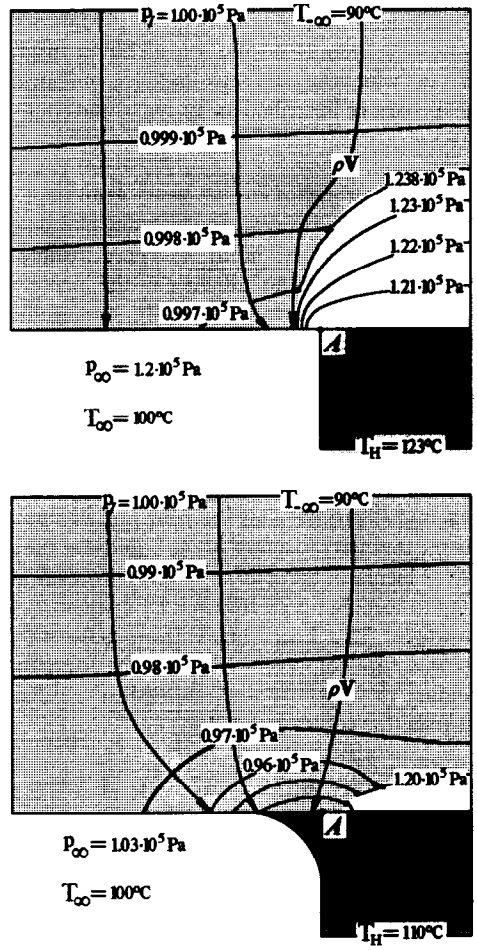

FIG. 4. The isobar and the lines of mass flux at $p_l = 1.00 \times 10^5$ Pa. $T_{-\infty} = 90$°C in cases: (a) $p_\infty = 1.20 \times 10^5$ Pa, $T_H = 123$°C and (b) $p_\infty = 1.03 \times 10^5$ Pa, $T_H = 110$°C.

further assumed that the heat transfer agent was supplied to the CS at the temperature $T_{-\infty}$ and the pressure p_l which varied correspondingly from 80 to 95°C and from 0.80×10^5 to 1.00×10^5 Pa. Thermal conductivity of the material in Ω_H corresponded to that of copper: $\lambda_H = 380$ W m^{-1} K^{-1}. The temperature T_H varied from 105 to 150°C. The pressure of vapour p_∞ at its discharge from the CS varied between 1.00×10^5 and 1.20×10^5 Pa, and its temperature T_∞ was assumed to be 100°C. The coefficient of convective transfer α was assumed to be 3×10^5 W m^{-2} K^{-1}. The calculations were performed for the cross-sections of the fragments of the CS and HIE: $OB \times OD = 200 \times 200$ μm^2 and $OA \times OE = 70 \times 70$ μm^2, respectively.

The results of the calculations are in part represented in Fig. 4 in terms of isobars and the mass flux lines, and in Fig. 5 in terms of isotherms and heat flux lines.

A series of calculations for different values of T_H [see equation (11)] allowed us to observe in detail the phases of the evolution of the process: the areas where

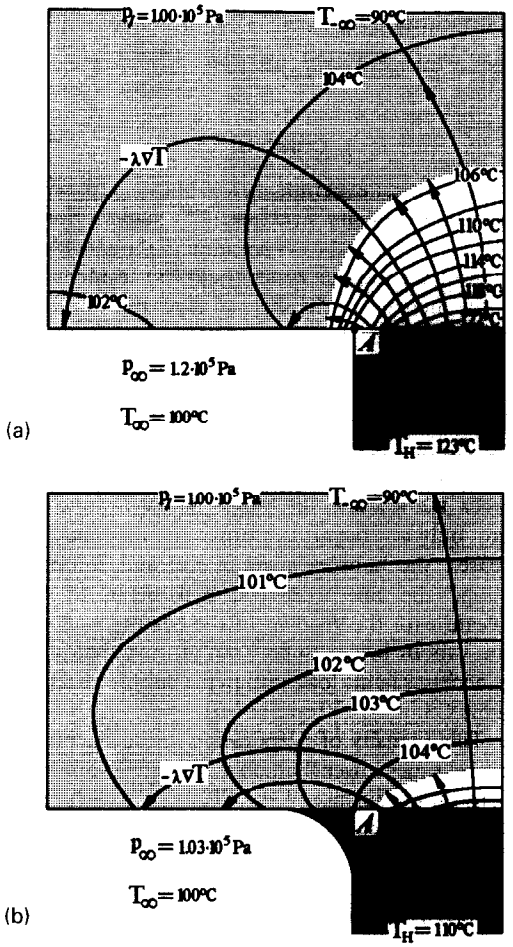

FIG. 5. Isotherms and heat flux lines at $p_l = 1.00 \times 10^5$ Pa, $T_{-\infty} = 90°C$ in cases (a) $p_\infty = 1.20 \times 10^5$ Pa, $T_H = 123°C$ and (b) $p_\infty = 1.03 \times 10^5$ Pa, $T_H = 110°C$.

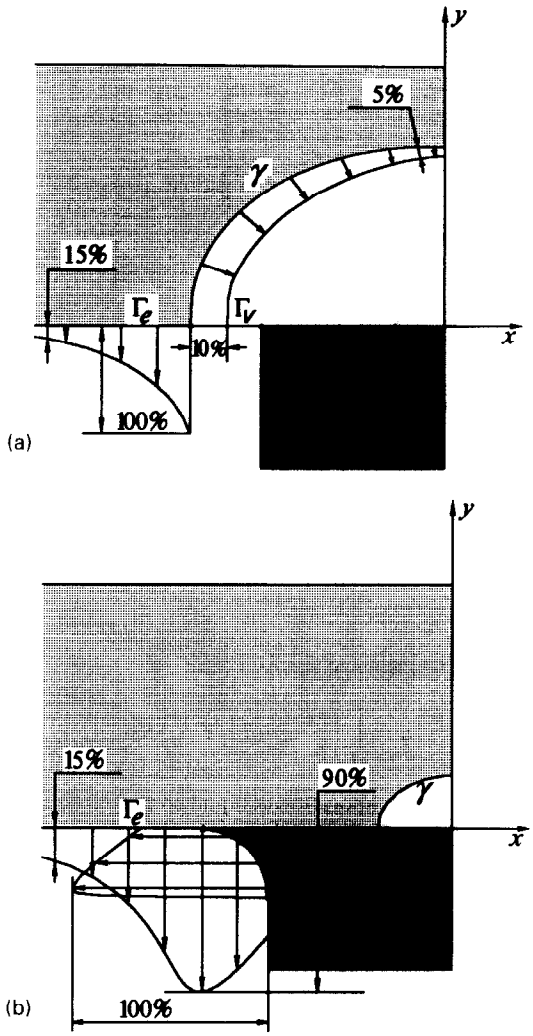

FIG. 6. Distribution of evaporation intensity.

the vapour zones in the CS originate, their growth and configuration for the increasing heat load, and to determine the areas of the most active evaporation.

It can be seen from Figs. 4 and 5 that for small heat loads the vapour zone is localized in the centre of the HIE. With the increase of the heat load the dried region expands and its base exceeds the area of contact of the interior of the CS. This peculiarity is caused by that fact that the rate of penetration of heat in the CS in the area of the contact turns out to be greater that the convective output of heat from the area to the place of evaporation. Indeed, the lines of the mass flux indicate that the heat transfer agent mostly flows around the vapour zone as though it were an obstacle. Hence, the convective movement inside the vapour zone is rather weak and weakens with the increase in size of the zone.

The character of the evaporation intensity distribution

$$I = \frac{\rho r K}{\mu} \frac{\partial p}{\partial v}$$

on the interphase boundary also shows (cf. Fig. 6) in the weakness of the convective motion inside the vapour zone. When meniscus is absent (Fig. 6a), this rate is several times smaller on γ than in Γ_e. This occurs because the removal of vapour from γ through the CS is hindered. The lighest intensity is observed in the neighbourhood of the point of contact between the boundaries γ and Γ_e, where the mass flux lines get thicker. The intensity on Γ_e drops abruptly with the distance because the heat source becomes remote.

The distribution of the intensity I in the presence of the meniscus is shown in Fig. 6(b), except for the distribution of I on the surface of the meniscus itself. Still, in Fig. 6(b) the distribution of the values

$$\frac{\rho r K}{\mu} \frac{\partial p}{\partial y} \quad \text{on} \quad \Gamma_x^m \quad \text{and} \quad \lambda_H \frac{\partial T}{\partial x} \quad \text{on} \quad \Gamma_y^m$$

is presented which reflect the filtration of liquid through Γ_x^m and the output of heat from Γ_y^m. These values characterize the intensity of evaporation from the surface of the meniscus.

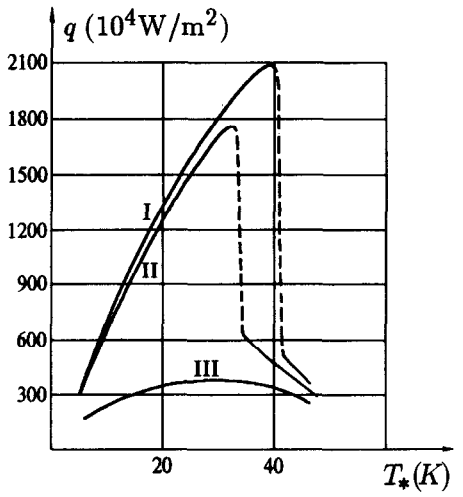

FIG. 7. Functional characteristics of the CS. Pressure drops corresponding to curves I, II, III are equal respectively to 0.03×10^5, 0.06×10^5 and 0.20×10^5 Pa.

The dependence of the heat flux

$$q = \int_{\Gamma_l} \frac{\rho r K}{\mu} \frac{\partial p}{\partial y} (T - T_{-\infty}) \, dx$$

consumed for evaporation of liquid coming in through the boundary Γ_l on the thermal action T_*, which is calculated as

$$T_* = \bar{T}_c - T_\infty,$$

where $\bar{T}_c$ is the integral average temperature on Γ_l, an important functional characteristic of the CS. A typical series of dependencies of $q = q(T_*)$ on the value of hydraulic actions $p_\infty - p_l$ is shown in Fig. 7. The heat flux q first increases as T_* grows and then drops. The maximum is attained at the value of T_* close to T_*^0, which corresponds to the transition from a 'small' to a 'large' vapour zone, i.e. to the situation when the base of the vapour zone coincides with the area of contact between the HIE and CS. In the case of small pressure drops $p_\infty - p_l$ (curves I and II) the heat flux q at $T_* < T_*^0$ (small vapour zone) is significantly greater than in cases of large pressure drops (curve III), because in the former case there occurs additional evaporation on the meniscus, while in the latter case the meniscus is practically absent. The causes of the decrease in q at $T_* > T_*^0$ are different at different hydraulic loads. When hydraulic loads are small, the transition to the regime of $T_* > T_*^0$ (large vapour zone) results in the destruction of the meniscus, and, therefore, in the elimination of the larger component of the total evaporation flux, which is characterized by an abrupt drop in the heat flux (the dashed lines of the curves I and II). When hydraulic loads are large (curve III), the decrease in the heat flux under large thermal actions (and, consequently, with the growth of distance between the evaporation section Γ_l and HIE) is connected with the growth of thermal resistance it has to overcome on its way from HIE to the evaporation section Γ_l.

5. CONCLUSION

Mathematical experiments in a heat pipe evolution zone with a capillary structure (CS) made it possible to observe in detail the evaporation of the process, the growth of the vapour zones (bubbles) inside the CS with the increase of the thermal load and to plot the corresponding patterns of isotherms and mass flux lines. We can assert the following:

1. There exists an area of stable thermal conditions when the interphase boundary enters inside the CS. First of all, this occurs at the places of direct contact between the CS and the bulges of the heating wall, where bubbles begin to form. As the heat load increases, the bubbles grow in size and completely envelope the microcontacts, and begin to communicate with the grooves of the heating wall. As a result, vapour begins to flow out of the bubbles. Further increases in the load lead to the bubbles extending into the CS.
2. The intensity of evaporation inside the bubbles is several times lower than on the nearby evaporation regions on the surface of the CS. Within each region the maximal intensity is observed at the points closest to the microcontact. The causes of the low intensity of evaporation inside the bubbles are large hydraulic losses occurring while vapour moves across the CS.
3. If there exists a meniscus, and under the assumption that the liquid in it is motionless, the evaporation flux from the meniscus exceeds that from the surface of the CS by two to three times. Actually (taking into account the movement of the liquid in the meniscus and the heat transfer inside it), the difference is even greater. Therefore, taking measures in order to create the conditions for the existence of a meniscus is quite expedient. In particular, it is necessary to diminish the pressure drop across the CS.

REFERENCES

1. Yu. V. Gerasimov and Yu. F. Maidanik, Heat pipe, A.s.449213 USSR (in Russian) B. I., N41 (1974).
2. A. S. Demidov, L. V. Petrina, V. Ja. Sasin and E. S. Jatsenko, Heat and mass transfer in the evaporation zone. *Trudy MEI* (in Russian) N173, 44–48 (1988).
3. A. S. Demidov and E. S. Jatsenko, Mathematical experiment on investigation of heat and mass transfer. In *Symposium on Heat Pipe Research and Applications*, Shanghai, China, p. 137 (1991).
4. A. S. Demidov and E. S. Jatsenko, Mathematical experiment on investigation of heat and mass transfer in the evaporation zone of a heat pipe. *Teplofizika vysokikh temperatur* (in Russian) **30**, 566–572 (1992).
5. E. W. Saaski, Investigation of an inverted meniscus heat pipe wick concept. NASA CR-137,724, Sigma Research, Inc., August (1975).
6. S. A. Kovalev, S. L. Solovjev and O. A. Ovodkov, Liquid boiling at porous surfaces. Heat- and mass-exchange processes at phase transformation and in two-phase

flows. *Proceedings of the International Seminar* (in Russian), Minsk, pp. 26–38 (1985).
7. A. S. Demidov, Uniqueness of solution for boundary value problems for an elliptic second-order equation with some conditions of conjugation on the surfaces of discontiuity of the coefficients. *Vestnik MGU* (Moscow State University) (in Russian) N3, 30–36 (1969).
8. Free Boundary Problems. *Proceedings of a Seminar held in Pavia*, Vols I, II, Rome (1980).
9. R. P. Fedorenko, Iteration methods for solution of difference elliptic equations. *Uspekhi Math. Nauk* (in Russian) 2, 121–171 (1973).
10. A. S. Demidov, Asymptotic of solutions of boundary value problems for a linear elliptic second order equation with 'flash' type coefficients. *Trudy Mosc. mathem. obshchestva* (in Russian) **23,** 77–112 (1970).
11. R. Courant, *Partial Differential Equations*. New York (1962).